Far field modeling of the plasma plume of a Hall thruster

Cite as: Journal of Applied Physics **92**, 1764 (2002); https://doi.org/10.1063/1.1492014
Submitted: 08 March 2002 . Accepted: 16 May 2002 . Published Online: 30 July 2002

Iain D. Boyd, and Rainer A. Dressler

Far field modeling of the plasma plume of a Hall thruster

Iain D. Boyd[a)]
Department of Aerospace Engineering, University of Michigan, Ann Arbor, Michigan 48109-2140

Rainer A. Dressler
Air Force Research Laboratory, Space Vehicles Directorate, Hanscom Air Force Base, Massachusetts 01731-3010

(Received 8 March 2002; accepted for publication 16 May 2002)

Hall thrusters are an attractive form of electric propulsion that are being developed and implemented to replace chemical systems for many in orbit propulsion tasks on communications satellites. One concern in the use of these devices is the possible damage their plumes may cause to the host spacecraft. Computer models of Hall thruster plumes play an important role in integration of these devices onto spacecraft as the space environment is not easily reproduced in ground testing facilities. In this article, a hybrid particle-fluid model of a Hall thruster plume is applied to model the SPT-100 thrusters used on the Russian Express satellites. The emphasis of the article is on making assessment of the model through direct comparison with measurements of ion current density and ion energy distributions taken on board Express spacecraft. A model for simulating atom–ion collisions is described. The sensitivity of the plume simulation results to various aspects of the physical modeling is investigated. The plume model is able to predict many of the most important characteristics of the measured data. © *2002 American Institute of Physics.*
[DOI: 10.1063/1.1492014]

I. INTRODUCTION

Hall thrusters are under development in several countries including the United States, Russia, Japan, and France. These electric propulsion devices typically offer a specific impulse of about 1600 s and a thrust of about 80 mN. These characteristics make them ideally suited for spacecraft orbit maintenance tasks such as north–south station keeping. Under typical operating conditions, at a power level of about 1.5 kW, a voltage of 300 V is applied between an external cathode and an annular anode. The electrons emitted from the cathode ionize the xenon propellant efficiently aided by magnetic confinement within an annular acceleration channel (creating an azimuthal Hall current). The ions are accelerated in the imposed electric field to velocities on the order of 17 km/s. New classes of Hall thrusters are being developed at low power (100 W) for use on microspacecraft, and at high power (25 kW) for spacecraft orbit raising.

As with any spacecraft propulsion device (chemical or electric), computer modeling is used to assess any interactions between the plume of the thruster and the host spacecraft. In the case of Hall thrusters, there are three particular spacecraft integration issues: (1) the divergence angle of these devices is relatively large (about 60°) leading to the possibility of direct impingement of high energy propellant ions onto spacecraft surfaces that may result in sputtering and degradation of material properties. Material sputtered from spacecraft surfaces in this way may ultimately become deposited on other spacecraft surfaces such as solar cells, causing further problems; (2) back flow impingement of ions caused by formation of a charge exchange plasma; and (3) the high energy ions created inside the thruster cause significant erosion of the walls of the acceleration channel (usually made of metal or a ceramic such as boron nitride) and the erosion products may expand out from the thruster and become deposited on spacecraft surfaces.

A number of Hall thruster plume models have been developed and are reviewed in a recent article by Boyd.[1] These models have been assessed against detailed experimental data taken in the plumes of a variety of Hall thrusters in ground-based vacuum chambers. For a 1.5 kW class Hall thruster, the lowest background pressure that can be obtained in vacuum chambers is about 10^{-6} Torr, which corresponds to an orbital altitude of about 185 km. Clearly, this represents a pressure that is orders of magnitude higher than that encountered in the operation of Hall thrusters in geostationary earth orbit. Another limitation of vacuum chambers concerns their size. Most Hall thruster plume measurements have been taken such that the maximum distance from the thruster that was probed was about 1 m.

The primary objective of this article is to assess a state-of-the-art Hall thruster plume model in terms of its predictions for realistic space conditions of the far field of the plume. The assessment is made meaningful by the recent, in-orbit, plume measurements of SPT-100 Hall thrusters taken on board the Russian Express spacecraft.[2] The outline of the article is as follows. First, an outline of the Express spacecraft and the plume measurements is provided. Then, a description is given of the hybrid particle-fluid plume model employed in this study. Details are provided of a model for simulating ion–atom collisions. Results consisting of comparisons between measured and computed data for ion current density and ion energy distributions are then presented and discussed. The sensitivity of the model predictions to

[a)]Electronic mail: iainbody@umich.edu

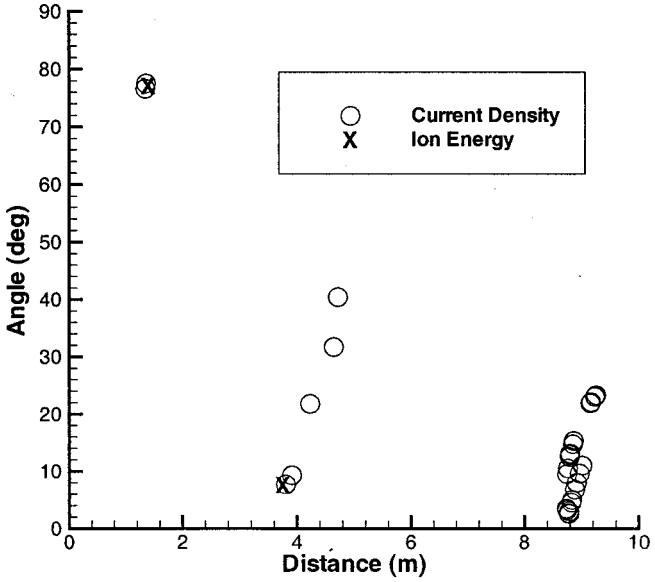

FIG. 1. Coordinates of the RPA sensors on the Express spacecraft that provided the data employed in the present study.

various physical modeling assumptions and boundary conditions is considered. The article closes with some conclusions and suggestions for further work.

II. EXPRESS FLIGHT DATA

A complete description of the two Russian Express-A satellites and the flight data collection program are provided by Manzella *et al.*[2] The thrusters employed on the spacecraft were SPT-100 models with a nominal thrust level of about 82 mN while operating at a discharge current of 4.5 A and a total flow rate (anode plus cathode) of 5.3 mg/s. In some ways, the use of SPT-100 thrusters for the first recording of in-orbit plume data is most appropriate as this thruster has received the most attention in terms of both laboratory studies[3–7] and computational analyses.[7–9] A variety of sensors were installed on board the two spacecraft to characterize the effects of firing the Hall thrusters on the spacecraft operation and environment. The instruments included electric field sensors, Faraday probes to measure ion current density, retarding potential analyzers (RPAs) to measure ion current and ion energy, and pressure sensors. In addition, disturbance torques on the spacecraft imparted by the Hall thruster plumes were recorded.

From all of the above, the present study focuses on the RPA data for ion current density and ion energy distributions. This is in part due to the overlap with ground-based measurements of these properties, the relatively good apparent fidelity of these data, and the lack of postflight reduction of much of the other data. The locations where RPA data were measured are plotted in Fig. 1 with respect to an origin in the thruster exit plane on the thruster centerline. The variation in location is due to the firing of eight different thrusters and the fact that some of the sensors could be moved. Note that some of the sensors were as much as 8.8 m away from the thruster which is well in to the far field region of the plume.

TABLE I. Properties at the exit of the SPT-100 Hall thruster.

Inner diameter (mm)	60
Outer diameter (mm)	100
Plasma density (m^{-3})	10^{17}–10^{18}
Neutral density (m^{-3})	10^{18}
Ion velocity (m/s)	17000
Neutral velocity (m/s)	300
Electron temperature (eV)	4–10
Ion temperature (eV)	1–4
Neutral temperature (K)	1000

III. THEORY

A. Hall thruster plume model

To understand the type of numerical approach required to accurately model Hall thruster plumes, it is informative to consider some of the basic physical characteristics of the flow exiting from the thruster. In Table I, typical values of some of the pertinent properties are listed at the thruster exit for the SPT-100. For these plasma densities, the Debye length is very small, on the order of 10^{-5} m, which indicates that the plume is charge neutral for a relatively large distance away from the thruster. At the same time, the collision mean free paths are very large, on the order of 1 m. These fundamental physical properties of the plume suggest that a kinetic approach is necessary that simulates both plasma and collision effects.

In this study, a hybrid particle-fluid model is employed. The particle in cell (PIC) method[10] is employed to model the plasma dynamics, and the direct simulation Monte Carlo method (DSMC)[11] is used to simulate the collision dynamics. In the following sections, these models are briefly outlined.

B. Plasma dynamics

The first efforts to use a combination of the PIC and DSMC methods to model the plumes of Hall thrusters were made by Oh *et al.*[7] and this approach has formed the basis for subsequent work.[8,12] In general, the PIC method accelerates charged particles through applied and self-generated electric fields in a self-consistent manner. In Ref. 7, based on the plasma jet physical properties, the ions are modeled as particles and the electrons as a fluid. The plasma potential is obtained by assuming quasineutrality, which allows the ion density to represent the electron density. By further assuming that the electrons are isothermal, collisionless, and unmagnetized, and that their pressure obeys the ideal gas law, $p=nkT$, the Boltzmann relation is obtained

$$\phi-\phi^*=\frac{kT}{e}\ln\left(\frac{n}{n^*}\right), \tag{1}$$

where n is the electron number density, $*$ indicates a reference state, ϕ is the plasma potential, k is Boltzmann's constant, T is the constant electron temperature, and e is the electron charge. The potential is then differentiated spatially to obtain the electric fields.

There are several limitations of this approach. First, experimental evidence[3,5] indicates that there is variation of the electron temperature in Hall thruster plumes. The variation

occurs mainly in the near field of the plume. At the thruster exit, the electron temperature has been reported to be as high as 10 eV[5] and in the far field typical values are 1–2 eV.[3] This creates a difficulty in the choice of T to be used in Eq. (1). A further difficulty with application of the Boltzmann relation to Hall thruster plumes is the possible effects of the magnetic field. The combination of permanent and electromagnets employed in Hall thrusters is designed to provide optimum device performance. However, some of the magnetic field may leak out into the plume of the thruster. The amount of this leakage will depend strongly on the Hall thruster type and configuration.

Despite these limitations, the simple Boltzmann relation is widely used and has produced remarkably good agreement with a number of different plume properties measured in vacuum chambers, see Ref. 1 for examples. This approach therefore forms the base line model for the present study. An alternative approach sometimes employed in plasma dynamics is to assume that the electrons behave adiabatically in which the pressure, density, and temperature are related by

$$\frac{p}{p^*}=\left(\frac{n}{n^*}\right)^{\gamma}=\left(\frac{T}{T^*}\right)^{\gamma/\gamma-1}, \tag{2}$$

where γ is the ratio of specific heats, and $*$ again indicates a reference state. Thus, changes in the electron temperature are related to changes in the electron density. Substitution of Eq. (2) into the electron momentum equation, assuming collisionless, unmagnetized electrons gives:

$$\phi-\phi^*=\frac{kT^*}{e}\frac{\gamma}{\gamma-1}\left[\left(\frac{n}{n^*}\right)^{\gamma-1}-1\right]. \tag{3}$$

Results computed with this adiabatic approach using $\gamma=5/3$ are compared to the base line solutions obtained with the Boltzmann relation.

C. Collision dynamics

The DSMC method uses particles to simulate collision effects in rarefied gas flows by collecting groups of particles into cells which have sizes of the order of a mean free path. Pairs of these particles are then selected at random and a collision probability is evaluated that is proportional to the product of the relative velocity and collision cross section for each pair. The probability is compared with a random number to determine if that collision occurs. If so, some form of collision dynamics is performed to alter the properties of the colliding particles.

There are two basic classes of collisions that are important in Hall thruster plumes: (1) elastic (momentum exchange); and (2) charge exchange. At first glance, based on the low number densities at the thruster exit, it appears that collisions are unimportant in Hall thruster plumes. However, it will be found in the discussion of results that these collisions have a profound effect on the Hall thruster plume structure even though the mean free path for all collisions is large. Two different approaches to modeling the ion–atom collision processes are followed. In the first, simple scattering laws are combined with analytical models and experimental measurements for the cross sections. In the second approach, the scattering is determined by detailed calculations.

1. Simple model

Elastic collisions involve only exchange of momentum between the participating particles. For the systems of interest here, this may involve atom–atom or atom–ion collisions. For atom–atom collisions, the variable hard sphere (VHS)[11] collision model is employed. For xenon, the collision cross section is

$$\sigma_{\mathrm{EL}}(\mathrm{Xe},\mathrm{Xe})=\frac{2.12\times10^{-18}}{g^{2\omega}}\,\mathrm{m}^2, \tag{4}$$

where g is the relative velocity, and $\omega=0.12$ is related to the viscosity temperature exponent. For atom–ion elastic interactions, the following cross section of Dalgarno, McDowell, and Williams[13] is employed:

$$\sigma_{\mathrm{EL}}(\mathrm{Xe},\mathrm{Xe}^+)=\frac{6.42\times10^{-16}}{g}\,\mathrm{m}^2. \tag{5}$$

The model of Ref. 13 predicts that the elastic cross section for interaction between an atom and a doubly charged ion is twice that for an atom and a singly charged ion. It should be noted that the model of Ref. 13 employs a polarization potential and therefore is only valid for low energy (a few eV) collisions. In all elastic interactions, the collision dynamics is modeled using isotropic scattering together with conservation of linear momentum and energy to determine the post-collision velocities of the colliding particles.[11]

Charge exchange concerns the transfer of one or more electrons between an atom and an ion. In the present resonant symmetric exchange case, this is a long-range interaction that involves a relatively large cross section in comparison to an elastic cross section as defined by Eq. (5). Charge exchange is an important mechanism in Hall thruster plumes because at the thruster exit plane, the atoms and ions have velocities that differ by almost two orders of magnitude (see Table I). While the ions have been accelerated electrostatically, the atoms remain at thermal speeds. Thus, charge exchange produces a slow ion and a fast atom. The slow ion is much more responsive to the electric fields set up in the plume and is easily pulled behind the thruster into the back flow region. Thus, the so-called charge exchange plasma is formed near the thruster exit. It is because we need to model the charge exchange behavior accurately that we go to the trouble of using the DSMC technique.

For singly charged ions, the following cross section measured by Pullins *et al.*[14] and Miller *et al.*[15] is used

$$\sigma_{\mathrm{CEX}}(\mathrm{Xe},\mathrm{Xe}^+)=[-23.30\log_{10}(g)+142.21]\times0.8423\times10^{-20}\ \mathrm{m}^2. \tag{6}$$

Also reported in Refs. 14 and 15 are charge exchange cross sections for the interaction where a doubly charged ion captures two electrons from an atom. These cross sections are less than a factor of 2 lower than the values for the singly charged ions at corresponding energies. In the present simple model, it is assumed that there is not transfer of momentum

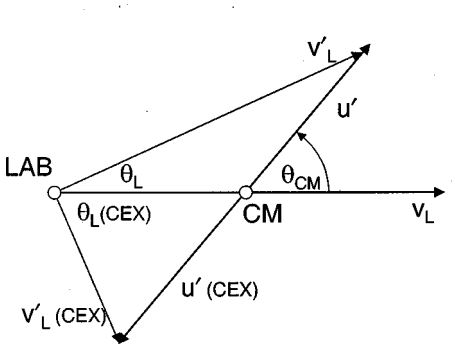

FIG. 2. Newton diagram of an elastic collision between a Xe ion and a Xe atom. LAB and CM are the laboratory and center-of-mass coordinate frame origins, respectively, v_L is the laboratory ion velocity, v_L' is the scattered laboratory velocity, u' are the CM scattered velocities, and CEX refers to charge-exchange scattering parameters.

accompanying the transfer of the electron(s). This assumption is based on the premise that charge exchange interactions are primarily at long range.

2. Detailed model

In this approach, the VHS model for Xe–Xe collisions is again employed along with isotropic scattering. The charge exchange collisions are based on the same measured cross sections, but scattering is modeled in detail with the notion that charge exchange is a subset of elastic scattering collisions. The determination of $Xe^+ + Xe$ differential cross sections was described in greater detail in an earlier article by Katz *et al.*[16] Figure 2 depicts a Newton diagram of an elastic Xe ion collision with a Xe atom. The Xe atom is assumed stationary at the origin of the laboratory (or spacecraft) coordinate system (LAB) and the ion is traveling at a LAB velocity, v_L. The collision results in a distribution of scattering angles with respect to the center of mass (CM), which can be approximately derived from the classical deflection function, $\Theta(E_T,b)$ (see Ref. 17, for example)

$$\Theta(E_T,b)=\pi-2b\int_{R_m}^{\infty}\frac{dR}{R^2[1-b^2/R^2-V(R)/E_T]^{1/2}}, \tag{7}$$

where E_T is the center-of-mass collision energy, b is the impact parameter, R is the interatomic distance, R_m is the trajectory turning point (point of nearest approach) and $V(R)$ is the interatomic potential energy. The deflection function is related to the center-of-mass scattering angle, θ_{CM}, through

$$\theta_{\mathrm{CM}}=|\Theta|,\ 0<\theta_{\mathrm{CM}}<\pi. \tag{8}$$

In the present symmetric collision system, the center-of-mass velocity is given by half the laboratory velocity. The differential cross section is obtained from

$$I(\theta_{\mathrm{CM}},E_T)=\frac{d\sigma}{d\Omega_{\mathrm{CM}}}=\left|\frac{b}{\sin(\theta_{\mathrm{CM}})d\theta_{\mathrm{CM}}/db}\right|, \tag{9}$$

where the solid angle, $d\Omega_{\mathrm{CM}}$, is given by $d\Omega_{\mathrm{CM}}=2\pi\sin\theta_{\mathrm{CM}}d\theta_{\mathrm{CM}}$. Conversion to the laboratory frame[16] yields

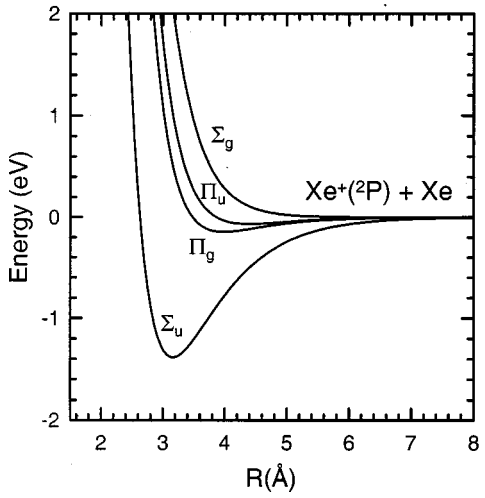

FIG. 3. Spin-orbit free Xe_2^+ potentials as calculated by Amarouche coworkers (see Ref. 18).

$$I(\theta_L)=\frac{d\sigma}{d\Omega_L}=\frac{d\sigma}{d\Omega_{\mathrm{CM}}}4\cos\theta_L. \tag{10}$$

Note, that the total flux into a particular solid angle can be the result of a superposition of multiple impact parameters, b, as a consequence of Eq. (7) and the shape of the interaction potential.

The calculation of the angular cross sections boils down to knowledge of the interaction potentials, validated by charge-exchange integral cross sections.[14,15] Classical differential cross sections are calculated using the averaged Xe_2^+ spin-orbit free potentials calculated by Amarouche, Durand, and Malreiu[18] and shown in Fig. 3. Note that the Π potentials have twice the weight of the Σ potentials. Thus, an elastic scattering trajectory occurs on one of two Π or Σ potentials with a probability of 2/3 and 1/3, respectively. In either case, the scattering can also involve charge exchange, which corresponds to a transition to the other potential of the respective *gerade-ungerade* (u,g) pair (e.g., a $\Sigma_g-\Sigma_u$ transition). The charge-exchange probability, $P_{\mathrm{CEX}}(b)$, is determined from[14]

$$P_{\mathrm{CEX}}(b)=\frac{1}{3}\sin^2\Delta_\Sigma+\frac{2}{3}\sin^2\Delta_\Pi, \tag{11}$$

where Δ_l is the difference in elastic scattering phase shifts for trajectories on the respective *gerade* and *ungerade* interaction potentials. Figure 4 displays $P_{\mathrm{CEX}}(b)$ for the potentials of Fig. 3 at an ion energy of 300 eV. At impact parameters less than 3 Å, the charge-exchange probability oscillates rapidly between 0 and 1. At impact parameters exceeding 5 Å, the charge-exchange probability is dominated by the stronger Σ interaction, and varies between 0 and about 1/3. From the deflection function, Eq. (7), averaged over all potentials, it is seen that at $b=3$ Å, the average scattering angle is about 2°. Consequently, $P_{\mathrm{CEX}}=0.5$ at scattering angles exceeding 2°, corresponding to smaller impact parameters. This assumption must be based on a solid angle of observance that averages over oscillations, which is definitely the case in the present space experiments. There is,

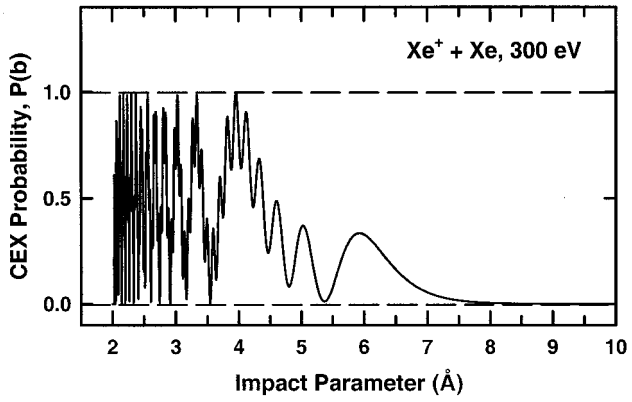

FIG. 4. Impact parameter dependence of the $Xe^+ + Xe$ charge-exchange probability at an ion energy of 300 eV. The probability is calculated using the potentials of Fig. 3.

therefore, an equal flux of ions scattered in opposite directions with respect to the center of mass (CM) i.e.

$$I_{\text{ion}}(\theta_{\text{CM}}) = \frac{1}{2} I(\theta_{\text{CM}}) + \frac{1}{2} I(\pi - \theta_{\text{CM}}). \tag{12}$$

Figure 5 shows the differential cross section $I_{\text{ion}}(\theta_{\text{LAB}}) = d\sigma/d\Omega_{\text{LAB}}$, representative of angular distributions with respect to the thruster axis, calculated for an ion energy of 300 eV. The calculations are performed for both inclusion and exclusion of charge exchange. The effect of charge exchange is most dramatic at large angles, as expected. Regarding the accuracy of the derived differential cross sections, it must be emphasized that the potentials, to which analytical expressions have been fit, are calculated in the vicinity of the chemical interaction region. However, large angle scattering depends on the interaction at very short interatomic distances, and are thus sensitive to the applied functional form representing the repulsive part of the potential. Experiments to verify the current cross sections would thus be of great value.

The differential cross sections computed by this approach without charge exchange are also shown as a normalized distribution in Fig. 6 as a function of scattering angle. This representation is useful for implementation in the

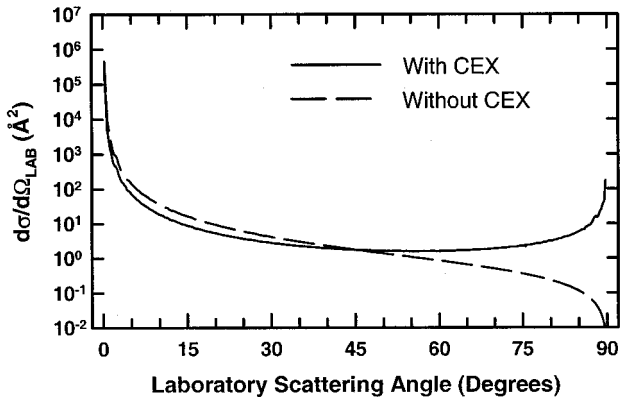

FIG. 5. Differential cross sections in LAB frame for 300 eV Xe^+ scattering in Xe with and without charge exchange.

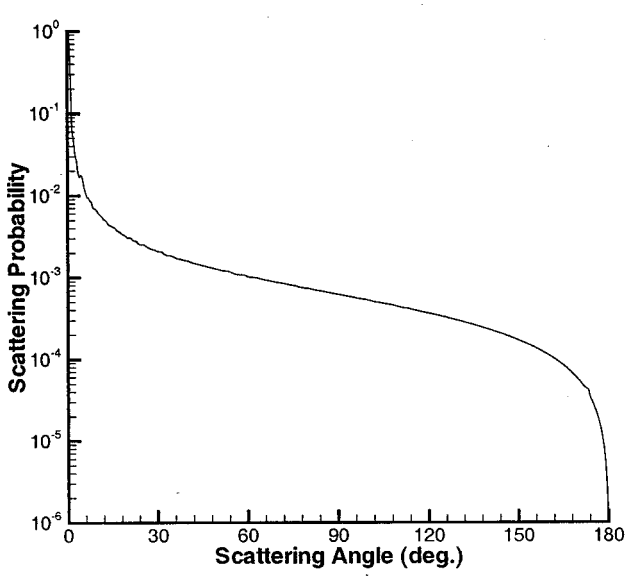

FIG. 6. CM distribution of scattering angle for $Xe-Xe^+$ interactions.

DSMC component of the model. These results indicate (as expected) that the majority of charge exchange interactions involve very low angle scattering. As discussed above, $P_{\text{CEX}} = 0.5$, and so the same scattering data are employed for atom–ion momentum exchange interactions. The cross section employed for these elastic collisions is the same as that for charge exchange that is again based on the experimental measurements of Refs. 14 and 15.

D. Boundary conditions

For PIC-DSMC computations of Hall thruster plumes, boundary conditions must be specified at several locations: (1) at the thruster exit; (2) along the outer edges of the computational domain; and (3) along any solid surfaces in the computational domain.

Several macroscopic properties of the plasma exiting the Hall thruster acceleration channel are required for PIC-DSMC computations. Specifically, the plasma potential, the electron temperature, and for each of the particle species we require the number density, velocity, and temperature. In the real device, these properties vary radially across the annular face of the thruster exit plane, and also, in many operating modes of the thruster, these quantities vary in time. In general, the approach to determining these properties is a mixture of analysis and estimation. By assuming ion and neutral temperatures (typically 4 eV and 1000 K, respectively) and using measured properties such as thrust, mass flow rate, and current, it is possible to determine the species number densities and velocities. This approach gives uniform profiles of all properties across the exit plane. Generally, a small half angle is imposed at the thruster exit plane to provide a variation in the velocity vector. An alternative approach considered here uses output from a two-dimensional PIC-MCC (Monte Carlo collision) model of the acceleration channel[19] as input to a PIC-DSMC plume computation.

Both field and particle boundary conditions are required at the outer edges of the computational domain. The usual

field conditions employed simply set the electric fields normal to the boundary edges equal to zero. For plume expansion into vacuum, the particle boundary condition is to remove from the computation any particle crossing the domain edge.

In all configurations, the solid exterior walls of the thruster must be included in the computation. In the present study, the potential of the walls is set to zero. Any ions colliding with the thruster walls are neutralized. Both atoms and neutralized ions are scattered back into the flow field from the surface of the thruster wall assuming diffuse reflection.

IV. RESULTS

The Hall thruster plume model described above is assessed by making direct comparison with ion current and ion energy distributions measured on board the Express spacecraft. The base line simulation is performed as follows: (1) at the thruster exit, the densities and temperatures are assumed to be radially uniform, the velocities are based on a divergence angle of 15°, an ion temperature of 4 eV is assumed, and the densities and velocities are obtained from the mass flow rate and integrated ion current; (2) the Boltzmann relation is used with a fixed electron temperature of 3 eV; (3) the ''detailed'' collision model is employed. The sensitivity of the model predictions to these assumptions is considered.

The computational domain extends more than 10 m axially from the thruster exit and 10 m radially from the thruster centerline to cover all of the Express probe locations. This is achieved using a mesh containing 190 by 175 nonuniform, rectangular cells. In a typical computation, approximately 4 million particles are employed with about 60% representing ions (both single and double charged). The neutral atom flow is first allowed to reach a steady state by using a large time step. The ions are then subsequently introduced with a time step of about 10^{-7} s. The computations reach a steady state for the ions after about 5000 iterations and solutions are then averaged over a further 10000 iterations. The total computation time is about 24 h on a personal computer. In Figs. 7 and 8, contours are shown of the ion and neutral atom number densities, respectively. These show that the two populations follow quite different plume expansion dynamics. The charge exchange plasma formed vertically above the thruster exit plane can be seen in Fig. 7.

A. Ion current density

Angular profiles of ion current density are shown in Fig. 9 in which the Express data are compared with two different profiles measured for the SPT-100 in vacuum chambers by Manzella and Sankovic[4] and King.[6] There are several important points to be noted in this plot. First, while the laboratory data were obtained at 1 m from the thruster, as shown in Fig. 1, this is not the case for the Express measurements. To try to simplify the data comparisons, the Express data are interpolated to values at 1 m from the thruster assuming a $1/r^2$ relation for the decay in ion current density with distance from the thruster. The accuracy of this relation will be considered later. The figure also indicates that there is considerable spread in the Express data. In some cases, for the same angular location, there is as much as an order of magnitude

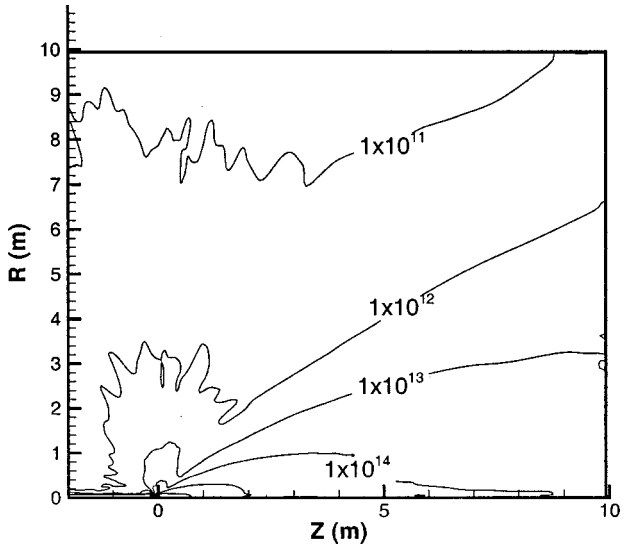

FIG. 7. Contours of ion number density (m^{-3}) for the base line computation.

variation. This illustrates the challenge in obtaining good quality plume data under in-orbit conditions. Thus, in general, it is not the aim of the modeling to agree exactly with the data, but rather the emphasis is on examining trends. Comparison of the three data sets in Fig. 9 shows the effect of the increased back pressure found in vacuum chamber experiments. As the back pressure is decreased from the King experiment, to the Manzella experiment, to the Express flight, the ion current density profile shows a significant decay at high angles. Close to the plume axis, the Express data are consistently a factor of 2–3 lower than the laboratory data. It is not clear whether this difference is real or part of a systematic error in the Express measurements. As noted earlier, the development and assessment of Hall thruster plume models has been performed exclusively using laboratory data. The Express data are the first set of measurements ob-

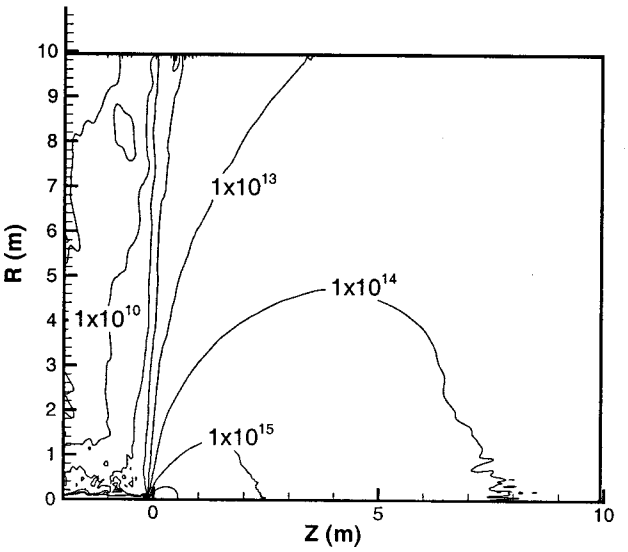

FIG. 8. Contours of neutral atom number density (m^{-3}) for the base line computation.

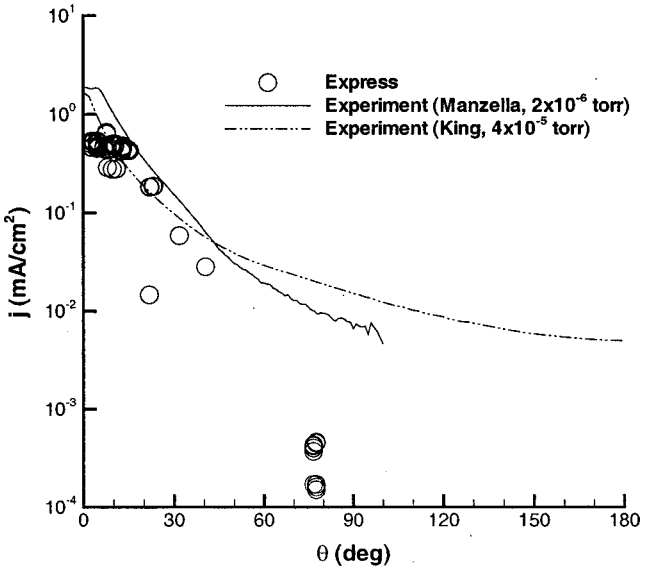

FIG. 9. Angular profiles of current density at 1 m from the thruster: comparison of flight and laboratory data.

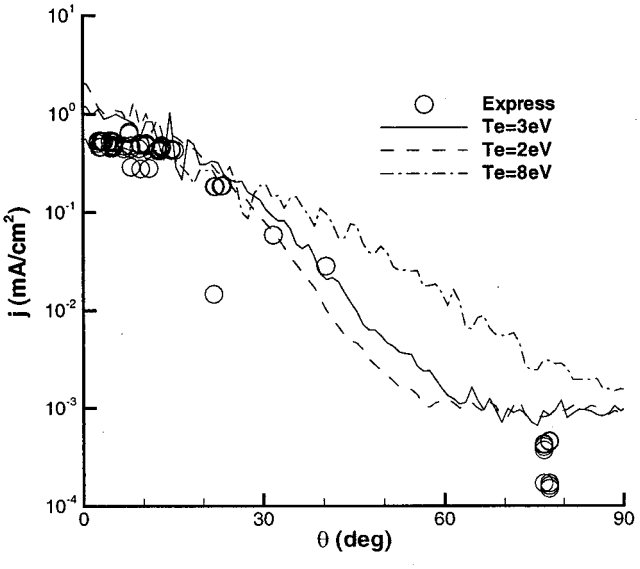

FIG. 11. Angular profiles of current density at 1 m from the thruster: effect of electron temperature.

tained in orbit for the plume of a Hall thruster. Comparisons of the models with laboratory plume data, Van Gilder, Boyd, and Keidar,[8] obtained excellent agreement between the data sets. One of the main questions to be answered in this study is whether these same models are able to predict the space-flight data.

In Fig. 10, angular profiles of ion current density are shown in which the Express data are compared to two profiles obtained from the same base line simulation. The Express data and a simulation profile obtained at 8.8 m from the thruster are each interpolated using the $1/r^2$ relation to 1 m from the thruster. The second simulation profile is obtained directly at 1 m from the thruster. Comparison of the two simulation results indicates that the ion current density does not exactly scale as $1/r^2$. At 8.8 m, the ion current density extrapolated to 1 m is a little lower at small angles and has a different overall shape in comparison to the actual 1 m result. It is believed that these differences are due primarily to collision effects. If there are no collisions in the plume, then the $1/r^2$ relation should hold for ion current density. However, the few collisions that do occur tend to scatter ions away from the axis leading to a relative reduction in ion current density there. Another important aspect concerns the effects of the electric fields that also change the ion dynamics from the simple scaling law. Therefore, in most of the simulation data shown in the remainder of this study, the plume data obtained at 8.8 m and scaled using the $1/r^2$ relation are shown rather than the data obtained directly at 1 m. It is interesting to note that the 8.8 m simulation profile appears to offer better agreement to the Express data at most angles.

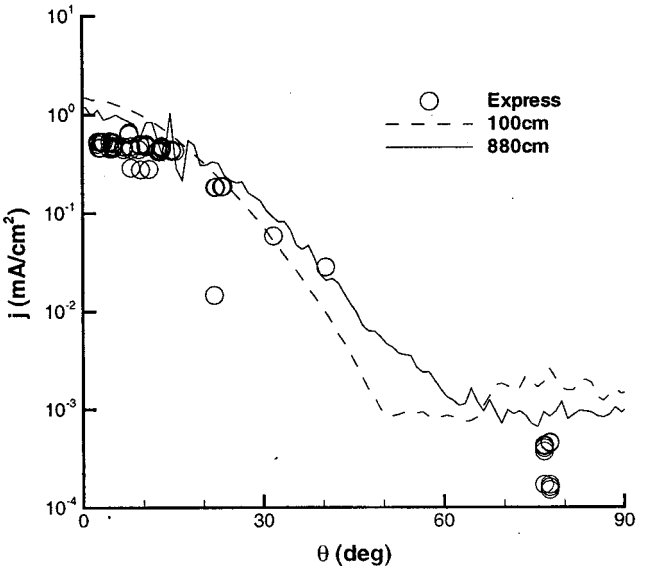

FIG. 10. Angular profiles of current density at 1 m from the thruster: comparison of model and flight data.

The effect of the fixed value of electron temperature in the simulation on the ion current density profiles is shown in Fig. 11. There is a consistent trend in which the profile becomes lower and flatter as the electron temperature increases. The value of 8 eV is chosen as this was employed in a plume model reported in Ref. 2. However, laboratory measurements of electron temperature indicate that this value is much too high except for a small region right at the thruster exit. In terms of the PIC-DSMC plume model, the value of 3 eV appears to offer the best agreement with the Express data.

The effect of the collision model on ion current density is examined next in Fig. 12. Simulation profiles obtained using the ''simple'' collision model at 1, 3.8, and 8.8 m from the thruster (with the latter two extrapolated to 1 m) are compared with the Express data. A very interesting effect is found in which the ion current density on the centerline decreases significantly with distance away from the thruster. After careful consideration of the flow field solutions for this case, it is found that the plasma beam emanating from the thruster first intersects the centerline and then ''reflects'' back from the centerline to continue as a beam angled away from the centerline. The angle of this beam is 15° which is exactly

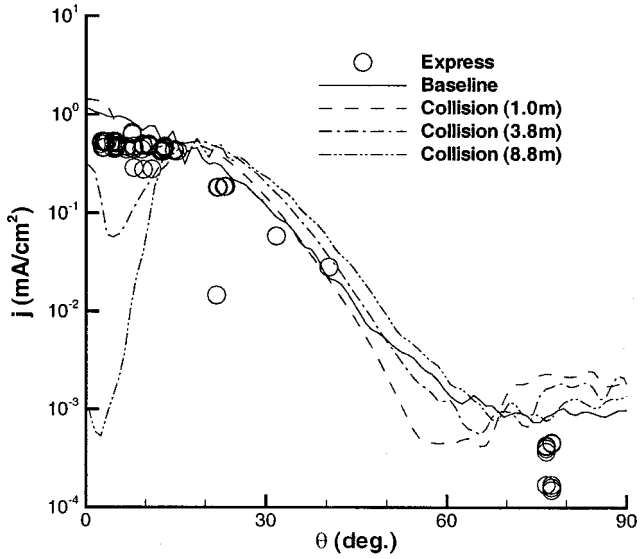

FIG. 12. Angular profiles of current density at 1 m from the thruster: effect of collision model.

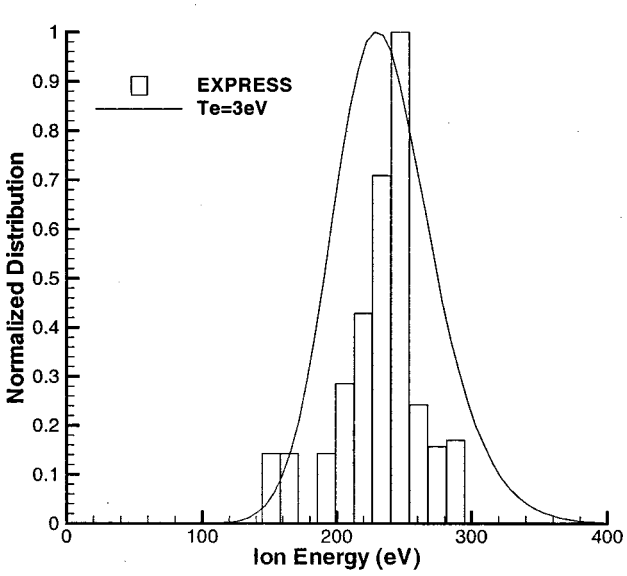

FIG. 14. Primary beam ion energy distribution function ($z=3.76$ m, $\theta=7.5°$).

the divergence angle imposed on the beam at the thruster exit plane. This behavior is not found with the detailed collision model and so indicates that the simple model does not randomize the plasma beam to nearly the same extent. This behavior with the simple collision model does not become apparent until distances beyond 1 m from the thruster are reached and so has not been noted in previous studies.

In Fig. 13, the effects are examined on ion current density of the properties assumed at the exit of the Hall thruster. The base line solution is compared with a simulation in which the exit profiles are obtained from a PIC-MCC simulation of the Hall thruster acceleration channel.[19] The PIC-MCC simulation predicts significant variation in all the ion and neutral atom flow properties across the thruster exit (see Ref. 19 for detailed discussion). The main point here is that the profiles employed in the results labeled "PIC-MCC" are significantly different from those employed in the other simulations. It is interesting to note, however, that the effects of these differences on the ion current density profile at 8.8 m from the thruster are quite small, with the main deviation occurring on the plume centerline where the PIC-MCC profile has a larger value. Finally, in terms of ion current density, use of the adiabatic electron model gives results that are essentially in agreement with those from the base line simulation.

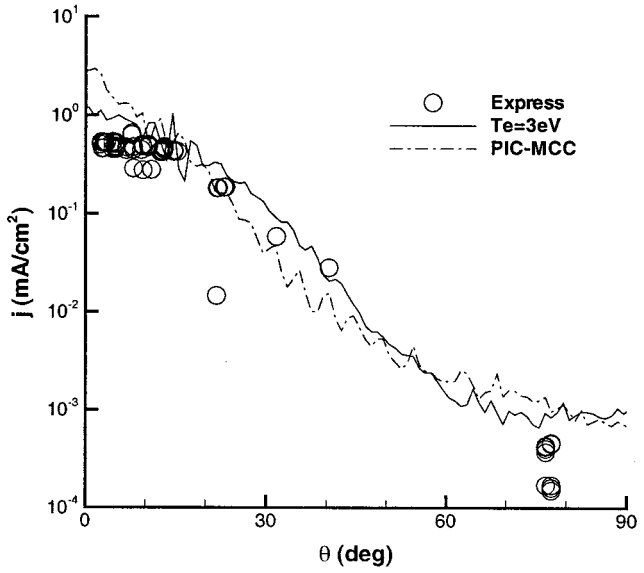

FIG. 13. Angular profiles of current density at 1 m from the thruster: effect of thruster exit profiles.

B. Primary beam ion energy distribution

The ion energy distribution in the primary beam near to the centerline (at 7° and at a distance of 3.76 m from the thruster) is considered. In Fig. 14, the Express data are compared with the results of the base line simulation. Recall that the base line ion temperature is 4 eV. Note, in terms of plotting style, that exact agreement between the data sets would mean that the solid line employed for the model results would go through the center of the horizontal bar of each column of the histogram used for the Express data. Ion energy distributions have been measured near centerline for the SPT-100 thruster in vacuum chambers by Myers and Manzella (using a RPA),[3] King [using a molecular beam mass spectrometer (MBMS)],[6] and Perot *et al.* (using an RPA).[20] Table II lists the full width at half maximum (FWHM) energy obtained in each of these experiments. Clearly, the RPA data measured in space indicate the narrowest distribution and this is perhaps explained by collisional broadening present in the vacuum tank experiments. Returning to Fig. 14, in general there is good agreement although the simulation distribution is clearly broader than the measured profile. The effect of the value of electron temperature assumed in the simulation is investigated in Fig. 15. A trend is observed

TABLE II. FWHM of ion energy distributions measured on centerline for SPT-100 thrusters.

Study	Instrument	FWHM (eV)	Angle (deg.)	Back pressure (Torr)
Myers and Manzella[a]	RPA	50	15	5×10^{-6}
King[b]	MBMS	40	0	4×10^{-5}
Perot *et al.*[c]	RPA	39	0	2×10^{-5}
Express[d]	RPA	33	7.5	Space

[a]Reference 3.
[b]Reference 6.
[c]Reference 20.
[d]Reference 2.

in which the peak of the distribution moves to higher ion energies as the electron temperature is increased. The width of the distribution is unchanged.

The effects on the simulation results of various aspects of physical modeling are shown in Fig. 16. Use of 1 eV for the ion temperature at the thruster exit leads to a narrower ion energy distribution that is closer to the Express data. Use of the simple collision model moves the peak of the distribution to a higher energy but does not change the width of the distribution. The movement of the distribution is assumed to occur as a result of the depletion of ion current density predicted by the simple model as shown in Fig. 12. This depletion leads to a stronger decay in ion density along the axis that in turn leads to stronger electric fields acting along the axis as a result of the Boltzmann relation. Although not shown here, it is found that use of the adiabatic model for the electrons gives an ion energy distribution that is identical to that obtained with the base line simulation.

Finally, in Fig. 17, the energy distribution obtained using the PIC-MCC results at the thruster exit is shown. This simulation shows good agreement with the width and shape of the measured distribution.

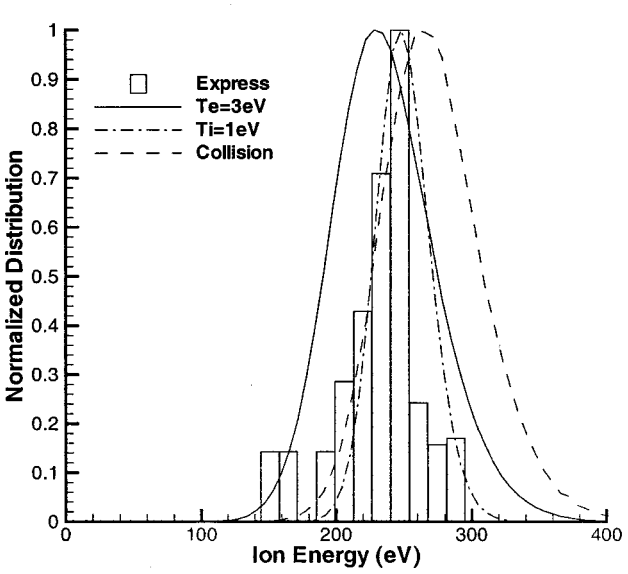

FIG. 16. Primary beam ion energy distribution function: effect of physical models.

C. Charge exchange ion energy distribution

The ion energy distribution obtained at the large angle of 77° (see Fig. 1) is now considered. This location is of interest since it is characterized primarily by charge exchange ions. Very few beam ions are expected to exit the Hall thruster at such large angles. In Fig. 18, the Express data are compared with the results from the base line simulation. Figure 18 illustrates a high energy structure measured on board the Express spacecraft that extends up to values associated with primary beam ions of about 260 eV. These high energies are not simulated by the model, although the peak of the distribution at about 28 eV is well predicted. King[6] measured the ion energy distribution function at 1 m from the SPT-100 from centerline to well behind the thruster including data collection at 80°. Unfortunately, the data at $\pm 80°$ are far

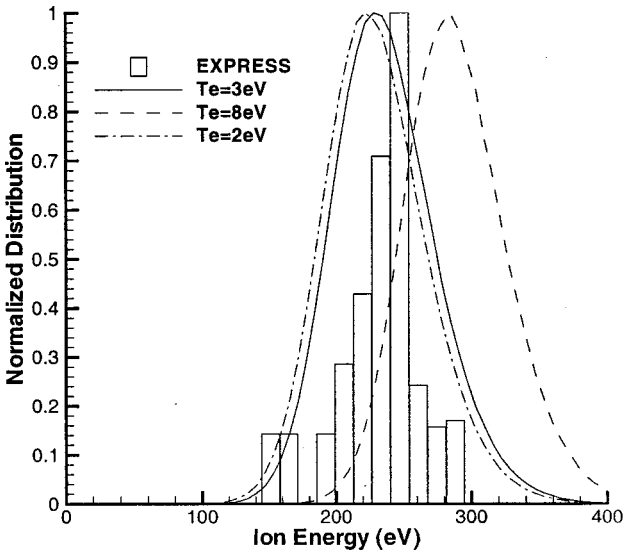

FIG. 15. Primary beam ion energy distribution function: effect of electron temperature.

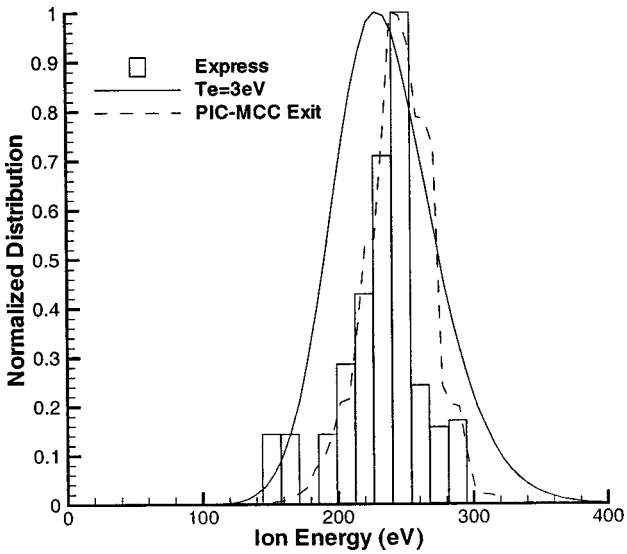

FIG. 17. Primary beam ion energy distribution function: effect of thruster exit profiles.

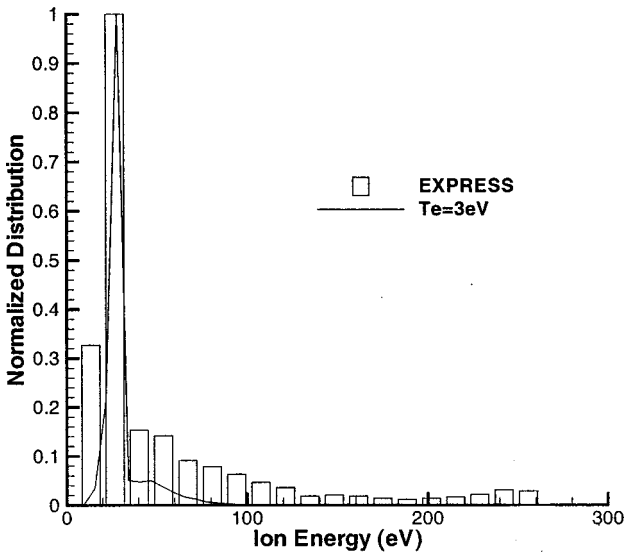

FIG. 18. Charge exchange ion energy distribution function ($z=1.40$ m, $\theta=77.5°$).

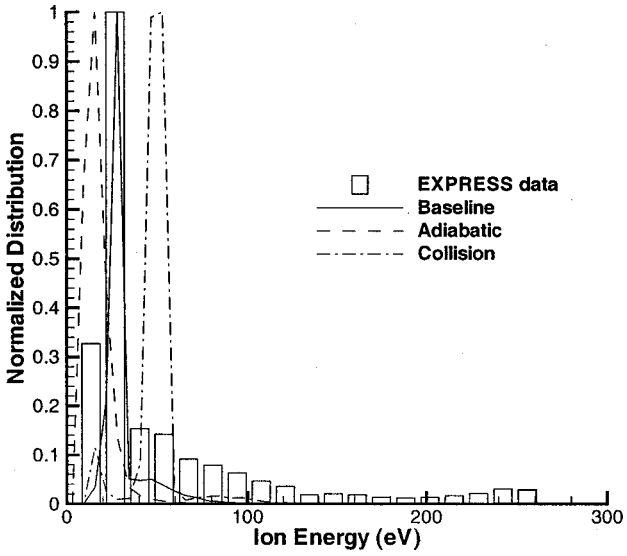

FIG. 20. Charge exchange ion energy distribution function: effect of physical models.

from identical and the MBMS diagnostic was not designed to detect the low energy ions measured by the Express RPA instrument.

The sensitivity of the model results to the electron temperature is investigated in Fig. 19. Increasing the electron temperature leads to the movement of the location of the peak of the distribution to higher ion energy. The value of 3 eV employed in the base line simulation provides the best agreement with the Express data.

Next, the effects of changing various aspects of the physical modeling employed in the simulations are considered. Specifically, the simple collision model and the adiabatic electron model are each employed in separate simulations. Figure 20 shows that the adiabatic model leads to a broader ion energy distribution with a peak at a lower ion energy. This indicates a smaller degree of ion acceleration with this model and is explained by the fact that for large regions of the plume, the adiabatic model predicts electron temperatures that are significantly lower than 1 eV. The effect of the simple collision model on the charge exchange plasma is to move the peak of the distribution to a significantly higher ion energy. This is again assumed to arise from the larger degree of ion scattering simulated for momentum exchange collisions with the simple model.

Finally, the effect of the Hall thruster exit plane profiles on the charge exchange plasma is shown in Fig. 21. The PIC-MCC profiles lead to an ion energy distribution that has the same peak as the base line simulation, with a broader distribution that agrees more closely with the Express data.

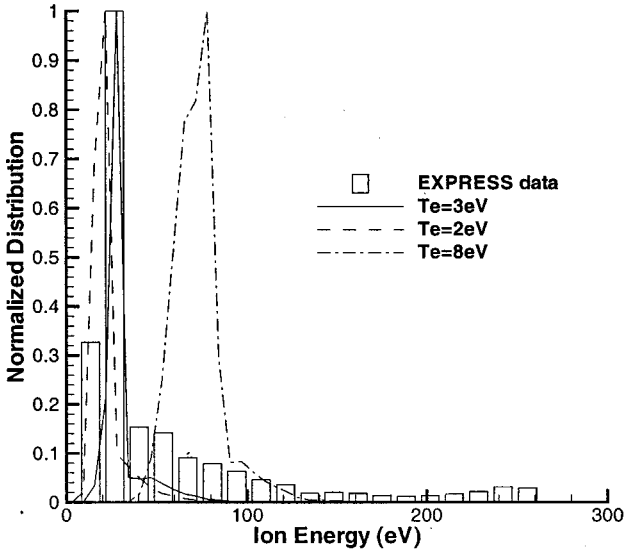

FIG. 19. Charge exchange ion energy distribution function: effect of electron temperature.

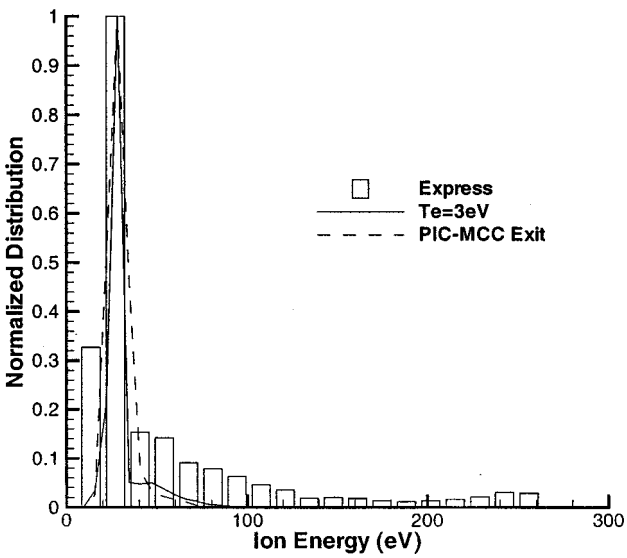

FIG. 21. Charge exchange ion energy distribution function: effect of thruster exit profiles.

V. CONCLUSIONS

A hybrid particle-fluid PIC-DSMC model has been applied to model the plume of an SPT-100 Hall thruster operating under the same conditions experienced on the Russian Express satellites. Assessment of the model was performed through direct comparison of predictions with ion current density and ion energy distribution functions measured in orbit on the Express spacecraft. These data are the first to be taken in the plume of a Hall thruster operated in space. Comparison of the simulation predictions with the data therefore allowed many fundamental aspects of the plume model to be assessed in the space environment. Specifically, the following components of the model were assessed (the approaches taken in the base line simulation are indicated in parentheses): (1) the value of electron temperature assumed in the Boltzmann relation (3 eV); (2) the collision model (detailed model); and (3) the properties at the thruster exit plane (uniform profiles with an ion temperature of 4 eV).

In general, the comparisons indicated that the base line plume model was able to capture most of the features found in the measured data. In terms of the ion current density profile, it was found from the simulation that the simple scaling law of $1/r^2$ for ion current density does not apply exactly as the plume expands far away from the thruster. Agreement within a factor of 2 of most of the flight data for ion current density was obtained at all angles for which data were measured. For the ion energy distribution measured in the primary ion beam, the base line simulation predicted the peak quite well, but the model distribution was significantly broader than the measured data. For the ion energy distribution measured in the charge exchange plasma, the base line simulation again correctly predicted the peak of the distribution, but provided a narrower profile and failed to simulate an extended high energy tail measured in space. For both ion energy distributions, a simulation performed using profiles at the thruster exit based on a separate PIC-MCC computation of the Hall thruster acceleration channel produced noticeably better results. It is therefore concluded that end-to-end simulations from inside the thruster to the plume far field are needed for accurate analysis of spacecraft integration issues for thrusters for which no flight data exist.

ACKNOWLEDGMENTS

The work of I.D.B. was funded in part by the TRW Foundation. The work of R.A.D. is supported by AFOSR under Task No. 2303EP02 (Program Manager: M. Berman). The authors are indebted to Dr. Mitat Birkan of AFOSR for additional support. The authors also thank David Manzella for providing the Express data in electronic form.

[1] I. D. Boyd, J. Spacecr. Rockets **38**, 381 (2001).
[2] D. H. Manzella, R. Jankovsky, F. Elliott, I. Mikellides, G. Jongeward, and D. Allen, IEPC 2001-044, 27th International Electric Propulsion Conference, Pasadena, CA, 2001.
[3] R. M. Myers and D. H. Manzella, IEPC 93-096, 23rd International Electric Propulsion Conference, Seattle, WA, 1993.
[4] D. H. Manzella and J. M. Sankovic, AIAA 95-2927, 31st AIAA/ASME/SAE/ASEE Joint Propulsion Conference and Exhibit, San Diego, CA, 1995.
[5] S. Kim, J. E. Foster, and A. D. Gallimore, AIAA 96-2972, 32nd AIAA/ASME/SAE/ASEE Joint Propulsion Conference and Exhibit, Orlando, Fl, 1996.
[6] L. B. King, Ph.D. thesis, University of Michigan, 1998.
[7] D. Y. Oh, D. E. Hastings, C. M. Marrese, J. M. Haas, and A. D. Gallimore, J. Propul. Power **15**, 345 (1999).
[8] D. B. Van Gilder, I. D. Boyd, and M. Keidar, J. Spacecr. Rockets **37**, 129 (2000).
[9] L. Garrigues, I. D. Boyd, and J. P. Boeuf, J. Propul. Power **17**, 772 (2001).
[10] C. K. Birdsall and A. B. Langdon, *Plasma Physics Via Computer Simulation* (Hilger, London, 1991).
[11] G. A. Bird, *Molecular Gas Dynamics and the Direct Simulation of Gas Flows* (Oxford University Press, Oxford, 1994).
[12] I. D. Boyd, J. Propul. Power **16**, 902 (2000).
[13] A. Dalgarno, M. R. C. McDowell, and A. Williams, Proc. Roy. Soc. **250**, 411 (1958).
[14] S. H. Pullins, Y. Chiu, D. J. Levandier, and R. A. Dressler, AIAA 00-0603, 38th AIAA Aerospace Sciences Meeting, Reno, NV, 2000.
[15] S. Miller, D. J. Levandier, Y. Chiu, and R. A. Dressler, J. Appl. Phys. **99**, 984 (2002).
[16] I. Katz, G. Jongeward, V. Davis, M. Mandell, I. Mikellides, R. Dressler, I. Boyd, K. Kannenberg, J. Pollard, and D. King, AIAA 2001-3355, 37th AIAA/ASME/SAE/ASEE Joint Propulsion Conference and Exhibit, Salt Lake City, UT, 2001.
[17] M. Child, *Molecular Collision Theory* (Academic, London, 1974).
[18] M. Amarouche, G. Durand, and J. P. Malrieu, J. Chem. Phys. **88**, 1010 (1988).
[19] I. D. Boyd, G. Garrigues, J. Koo, and M. Keidar, AIAA 2000-3520, 30th AIAA/ASME/SAE/ASEE Joint Propulsion Conference and Exhibit. Huntsville, AL, 2000.
[20] C. Perot, N. Gascon, S. Bechu, P. Lasgorceix, M. Dudeck, L. Garrigues, and J. P. Boeuf, AIAA 99-2716, 29th AIAA/ASME/SAE/ASEE Joint Propulsion Conference and Exhibit, Los Angeles, CA, 1999.